

# Axis-Aligned Document Dewarping

Chaoyun Wang<sup>1</sup> I-Chao Shen<sup>2</sup> Takeo Igarashi<sup>2\*</sup> Nanning Zheng<sup>1</sup> Caigui Jiang<sup>1\*</sup>

<sup>1</sup>National Key Laboratory of Human-Machine Hybrid Augmented Intelligence,  
National Engineering Research Center for Visual Information and Applications,  
Institute of Artificial Intelligence and Robotics, Xi'an Jiaotong University, China

<sup>2</sup>The University of Tokyo, Japan

chaoyunwang@stu.xjtu.edu.cn, jdilyshen@gmail.com, takeo@acm.org,  
nzheng@mail.xjtu.edu.cn, cgjiang@xjtu.edu.cn

## Abstract

Document dewarping is crucial for many applications. However, existing learning-based methods primarily rely on supervised regression with annotated data without leveraging the inherent geometric properties in physical documents to the dewarping process. Our key insight is that a well-dewarped document is characterized by transforming distorted feature lines into axis-aligned ones. This property aligns with the inherent axis-aligned nature of the discrete grid geometry in planar documents. In the training phase, we propose an axis-aligned geometric constraint to enhance document dewarping. In the inference phase, we propose an axis alignment preprocessing strategy to reduce the dewarping difficulty. In the evaluation phase, we introduce a new metric, Axis-Aligned Distortion (AAD), that not only incorporates geometric meaning and aligns with human visual perception but also demonstrates greater robustness. As a result, our method achieves SOTA results on multiple existing benchmarks and achieves 18.2%~34.5% improvements on the AAD metric.

## 1. Introduction

The digitization of documents dramatically facilitates our lives by converting information on physical documents into electronic data that can be used with digital devices. However, due to paper deformation, scanners must be fixed in position for precise scanning and acquisition, so this method has specific limitations. With the widespread use of mobile phones and cameras, photography has become a primary tool for digitization. Nonetheless, images taken by handheld cameras often suffer from geometric distortions and uneven lighting, negatively impacting the user's reading experience and downstream tasks like optical character

recognition (OCR).

In early research, many studies defined this problem as surface reconstruction from different imaging devices, including multi-view images [19, 33], stereo cameras [34], and structured light cameras [1, 26]. After that, some studies have leveraged document priors in single-view images to conduct extensive research, such as document boundaries [2], text lines [13, 14]. However, these are affected by the low-level features of the detected prior knowledge.

In the years of the flourishing development of deep learning, convolutional neural networks began to learn 2D deformation field mapping from deformed images to expected dewarping results [5, 7, 8, 12, 16, 17, 23, 24, 39, 41]. Data-driven methods perform supervised learning dewarping under the guidance of various supervision signals with synthetic annotations [17, 23, 36], such as depth [5], geometric semantics [25], control points [36, 40, 41], layout [17].

Although prior methods perform well on simple deformations, they often fail on document images with complex deformations. This is mainly because previous studies rely on strong supervision signals, such as control points, which are effective but have no geometric meaning, and text lines, which are meaningful but difficult to extract and lack generalization. These studies do not effectively use the inherent geometric information in the paper documents, which is investigated and exploited in this paper.

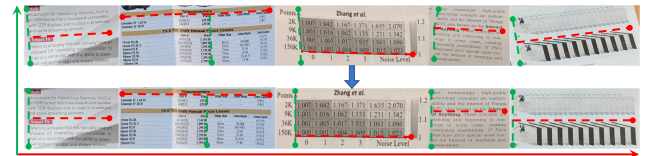


Figure 1. The top row is the warped local document image, and the bottom is the expected dewarping result. The main change feature is that the feature line aligns with the axis as much as possible. The dotted lines are added for better visibility.

\*Corresponding authors

In this paper, we perform document dewarping using a lightweight convolutional neural network that predicts a 2D unwarping grid from the distorted image. On this basis, to make the network better learn the nature of document dewarping, as shown in the dewarping example in Fig. 1, we expect the feature lines in the dewarped document to be more horizontally or vertically aligned. We leverage the inherent axis alignment property of the discrete grid geometry in planar documents, design a corresponding axis-aligned geometric constraint, and integrate it into the network training process. This dramatically improves the dewarping performance of the network. In the inference stage, to improve the dewarping performance for images containing target documents in different proportions and rotation angles, we propose an axis alignment preprocessing strategy. This strategy simplifies the dewarping process by leveraging the position properties of grid points and the axis alignment properties of planar document geometry. In the evaluation stage, we propose a new evaluation metric, AAD, to automatically measure the axis alignment distortion of the dewarped results, which have specific geometric meaning and align with human visual perception.

Our contributions are as follows.

- We introduce an axis-aligned geometric constraint, significantly enhancing the performance of learning-based document dewarping.
- We propose an axis alignment preprocessing strategy in the inference phase which boosts the dewarping performance robustly.
- We propose a new evaluation metric, AAD, that not only incorporates geometric meaning and aligns with human visual perception but also demonstrates enhanced robustness.

## 2. Related Work

Current research on document dewarping can be broadly categorized into traditional optimization methods and deep learning-based methods. As mentioned in the Sec. 1, traditional approaches to document dewarping primarily involve image processing and 3D reconstruction, preceding the advent of deep learning.

The research on image processing is to model the most commonly used low-level features extracted from document images, including letters/words, boundaries, spacing, and text lines, and to correct perspective and page curl distortion through local line spacing and cell shape, which can be formulated as an energy minimization optimization problem [14, 30, 31, 35]. In the recent research, Jiang et al. [12] applied deep learning to extract boundaries and document lines, followed by geometric constraint optimization. However, it is not easy to detect and perceive low-level features in deformed document images, which limits the application of methods based on image processing.

In 3D reconstruction research, variations in shadows from a single image or across different imaging devices, along with other input cues, have been utilized to reconstruct 3D surfaces [9, 19, 32, 37, 43]. Some studies model these surfaces as special types, such as cylindrical surfaces [3] and developable surfaces [26]. Recently, Luo et al. [22] treat the document as a developable surface and employ a recently proposed isometric constraint for modeling [11]. However, these methods rely on detecting document feature lines, resulting in long optimization times and limited generality.

In the research of deep learning, the current research has generated a large amount of data using rendering techniques and dataset collection, such as Doc3D [5], Inv3D [10], Simulated paper [17], UVDoc [36]. These data-driven approaches can be categorized into forward mapping methods [12, 18, 23] and backward mapping methods [5–8]. To further improve optimization, some methods incorporate additional supervision signals, such as text lines, masks, boundaries, layouts, angles, and curvatures to further improve optimization [4, 7, 16, 17, 42]. However, extracting these additional cues can introduce extra noise and lack generalizability.

An effective approach is to fully exploit the inherent geometric properties of the document, which are independent of annotated labels and generally more robust. As Xie et al. [39] exploited the continuity property of document deformation by incorporating local fairing constraints into the displacement prediction process. Furthermore, the recent GSO-Net [38], based on grid surface modeling, achieves accurate and robust optimization by learning the intrinsic geometric properties.

In this paper, we study and leverage the intrinsic geometric properties for document dewarping.

## 3. Method

We adopt the convolutional neural network architecture from UVDoc [36] as the foundation for our document dewarping network. This fully convolutional deep neural network simultaneously predicts the document’s 3D grid mesh and corresponding 2D unwarping grid in a dual-task framework, which is inspired by the work of Wang et al. [39, 40]

In the following sections, Sec. 3.1 details the axis-aligned geometric constraint introduced during training, Sec. 3.2 analyzes the loss functions employed during network training, and Sec. 3.3 describes the preprocessing strategy for axis alignment during inference.

### 3.1. Axis-Aligned Geometric Constraints

Fig. 2 illustrates the pipeline for computing the axis-aligned geometric constraint loss during training. Our approach takes advantage of the inherent geometric properties of planar paper, where the corresponding discrete grid geometry

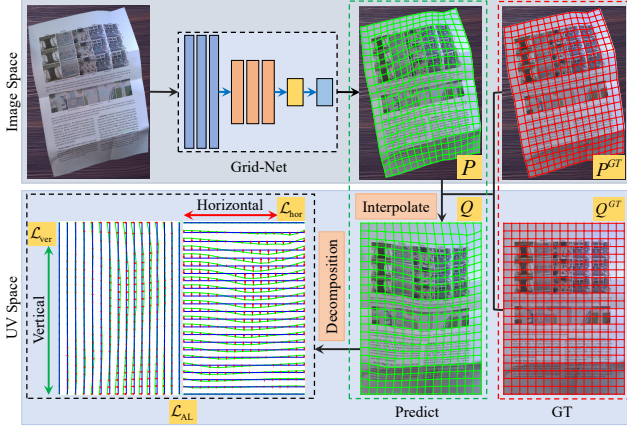


Figure 2. Axis-aligned geometric constraints were enforced during document dewarping network training. The top row shows the predicted 2D unwarping grid (obtained from Grid-Net in UVDoc [36]), and the bottom row displays its transformation into UV space based on the ground truth, facilitating the computation of the corresponding axis-aligned geometric constraints loss along horizontal and vertical directions.

is aligned along the horizontal and vertical axes (as shown by  $Q^{GT}$  in Fig. 2). This property aligns with the horizontal and vertical orientations of the document’s feature lines in image space. So, we can assess the axis alignment distortion of these feature lines in the dewarped image by computing the corresponding deviation of the unwrapped grid in planar space. However, since the current predictions are in image space, directly calculating this error is challenging.

To address this issue, we first employ an interpolation function to map the predicted 2D unwarping grid from image space  $P$  to UV space  $Q$ . In the UV space, the deviation from horizontal and vertical alignment is effectively quantified by computing the position variance along each row and column. By integrating these axis-aligned geometric constraints into the training process, we can guide the network in learning to dewarp distorted document feature lines toward the axis-aligned direction. The following are the details.

Given a distorted document image, a deep convolutional network predicts a 2D unwrapped grid points with sizes  $h \times w \times 2$ . Each point on the grid can be represented as:

$$P = \{p_{i,j}\}_{i=1,j=1}^{h,w}, \quad p_{i,j} = (x_{i,j}, y_{i,j}). \quad (1)$$

During training, the corresponding ground truth grid is:

$$P^{GT} = \{p_{i,j}^{GT}\}_{i=1,j=1}^{h,w}, \quad p_{i,j}^{GT} = (x_{i,j}^{GT}, y_{i,j}^{GT}). \quad (2)$$

In UV space, these ground truth grid are a uniform grid:

$$Q^{GT} = \{q_{i,j}^{GT}\}_{i=1,j=1}^{h,w}, \quad q_{i,j}^{GT} = (u_{i,j}^{GT}, v_{i,j}^{GT}). \quad (3)$$

To quantify the distortion of the prediction results, we distort the correspondence points in  $Q^{GT}$  according to the relative grid-position relationships in image space:

$$q = f(p) = \text{Interpolate}(q^{GT}; p^{GT}, P) \quad (4)$$

Thus, each predicted 2D grid point is transformed into the UV space as follows:

$$Q = \{q_{i,j}\}_{i=1,j=1}^{h,w}, \quad q_{i,j} = f(p_{i,j}) = (u_{i,j}, v_{i,j}). \quad (5)$$

In UV space, the axis-aligned error of 2D grid  $Q$  consists of two components. The horizontal error is quantified by the variance of the  $v$  values along each row, and the vertical error by the variance of the  $u$  values along each column, computed as follows:

$$\mathcal{L}_{\text{hor}} = \sum_{j=1}^h \text{Var}(\{v_{1,j}, v_{2,j}, \dots, v_{w,j}\}), \quad (6)$$

$$\mathcal{L}_{\text{ver}} = \sum_{i=1}^w \text{Var}(\{u_{i,1}, u_{i,2}, \dots, u_{i,h}\}). \quad (7)$$

The overall axis-aligned geometric constraint loss is then defined as:

$$\mathcal{L}_{\text{AL}} = \mathcal{L}_{\text{hor}} + \mathcal{L}_{\text{ver}}. \quad (8)$$

Minimizing  $\mathcal{L}_{\text{AL}}$  means the predicted 2D unwarping grid after being mapped into the UV space, as much as possible to align with the axis. Thus, the feature lines on distorted image dewarping results are axis-aligned as much as possible.

### 3.2. Loss Function

Let  $I \in \mathbb{R}^{H \times W \times 3}$  be the input image. The network predicts 2D unwarping grid  $G_{2D} \in \mathbb{R}^{h \times w \times 2}$  and corresponding 3D grid mesh  $G_{3D} \in \mathbb{R}^{h \times w \times 3}$ . The dewarped image  $I_d$  is obtained via an interpolation and grid sampling using  $I$  and  $G_{2D}$ . Our overall training loss is composed of the following components:

**Grid 2D and 3D Losses.** Following UVDoc [36], we supervise the network with the losses:

$$\mathcal{L}_{2D} = \|G_{2D} - G_{2D}^{\text{gt}}\|_1, \mathcal{L}_{3D} = \|G_{3D} - G_{3D}^{\text{gt}}\|_1 \quad (9)$$

where  $G_{2D}^{\text{gt}}$  and  $G_{3D}^{\text{gt}}$  denote the ground truth 2D grid and 3D coordinates, respectively.

**Axis-Aligned Geometric Constraint Loss.** We impose axis-aligned geometric constraints  $\mathcal{L}_{\text{AL}}$  in the UV space, guiding the network to achieve effective axis alignment dewarping of feature lines, as depicted in Sec. 3.1.

**SSIM Loss.** Since geometric dewarping may introduce artifacts (e.g., shadows) in the dewarped images, a pixel-level MSE loss might over-constrain model optimization and lead to instability. Hence, we incorporate an SSIM (Structural Similarity Index Measure) loss to measure the similarity between the dewarped image and the ground

truth, capturing both local structure and global consistency, which helps the model converge effectively:

$$\mathcal{L}_{SSIM} = 1 - SSIM(I, I_d). \quad (10)$$

The overall loss is defined as:

$$\mathcal{L}_{all} = \alpha \mathcal{L}_{2D} + \beta \mathcal{L}_{3D} + \gamma \mathcal{L}_{AL} + \lambda \mathcal{L}_{SSIM}. \quad (11)$$

with hyperparameters set as  $\alpha = \beta = 1, \gamma = 0.2, \lambda = 0.05$ , in our experiments.

### 3.3. Axis Alignment Preprocessing for Inference

During inference, previous methods employ additional segmentation and deformation models for preprocessing [7, 24] to improve dewarping robustness under diverse input conditions. Essentially, these methods distinguish between the background and the document region, enabling the model to focus on the document area and reducing dewarping difficulty. However, they do not directly address the elimination of geometric distortion.

Drawing on the insights from Fig. 1, axis alignment is central to the dewarping process. So, we propose an axis alignment preprocessing strategy, as illustrated in Fig. 3. For a given input image, we first compute the minimum-area rotation rectangle using the positional information from the predicted 2D unwarping grid. Subsequently, we perform an axis alignment rotation and clip the target area to obtain a preprocessed result. We then reapply the inference process on this preprocessed image to yield a refined dewarping outcome. If necessary, this process can be iteratively repeated to achieve further improvement under varying conditions. As shown in Fig. 3, the fine results obtained after preprocessing outperform the coarse results, effectively reducing the influence of the target position on the overall correction.

In contrast to previous preprocessing methods [7, 24], our approach eliminates the need for additional segmentation or deformation models. Instead, it directly leverages the predicted 2D unwarping grid to extract object region information, rendering the method more efficient and streamlined. A detailed analysis is provided in Sec. 4.5.

## 4. Experiments

The experimental section introduces the training data, test benchmarks, evaluation metrics, and implementation details, subsequently, we analyze the experimental results both quantitatively and qualitatively.

### 4.1. Datasets and Benchmarks

#### 4.1.1. Training Datasets

We used two datasets, Doc3D [5] and UVDoc [36], for alternative optimization models following the setting of Verhoeven et al. [36].

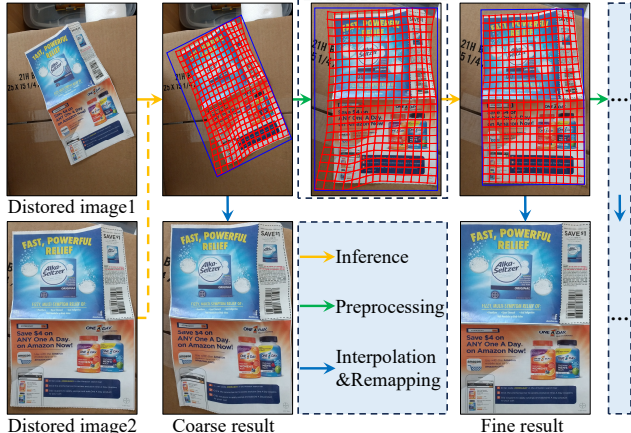


Figure 3. Illustration of the dewarping inference process with axis alignment preprocessing. The red grid represents the predicted 2D unwarping grid, while the blue rectangle indicates the minimum-area rotated rectangle computed from it.

Doc3D [5] is the largest distortion dewarping dataset, containing 100K distorted images. It was created using approximately 4,000 authentic document images and rendering software. The labels for each distorted document image include 3D coordinate maps, albedo maps, normals, depth maps, UV maps, and backward mapping maps.

UVDoc [36] aims to reduce the domain gap between the synthetic Doc3D dataset [5]—commonly used for training document unwarping models—and real document photographs. This dataset contains 20K pseudo-photorealistic document images and provides all the necessary information to train a coarse grid-based document unwarping neural network.

#### 4.1.2. Benchmarks

We evaluated our method on the following three benchmarks:

**DocUNet [23]:** This benchmark comprises 130 distorted images captured in natural scenes using mobile devices. Following previous methods, 25 rich-text images were selected for OCR evaluation, and according to DocGeoNet [8], the 127th and 128th images (which did not match the labels) were rotated by 180°.

**DIR300 [8]:** Captured with a moving camera, this benchmark contains 300 images of real distorted documents with complex backgrounds, varying degrees of distortion, and diverse lighting conditions. In line with previous studies, 90 rich-text images were selected for OCR evaluation.

**UVDoc [36]:** Generated via a pseudo-photorealistic rendering pipeline, this benchmark consists of 50 images, including matching pairs with and without illumination. Following the UVDoc protocol, 20 rich-text images were selected for OCR evaluation.

## 4.2. Evaluation Metrics

We evaluate our approach using image similarity metrics and optical character recognition (OCR) performance.

**MS-SSIM, LD and AD.** Following Ma et al. [23], we employ multi-scale structural similarity (MS-SSIM) and local distortion (LD) to assess image similarity. Additionally, we use the aligned distortion (AD) metric introduced in [24] to overcome the limitations of earlier measures.

**CER and ED.** Consistent with previous work, we measure OCR performance using Character Error Rate (CER) [27] and Edit Distance (ED) [15]. Our experiments utilize OCR recognition with Tesseract v5.4.0.20240606 and PyTesseract v0.3.13<sup>1</sup>.

Subsequently, we introduce the newly proposed metric.

### 4.2.1. AAD Metric

As illustrated in Fig. 1, our visual evaluation of document dewarped primarily relies on the axis alignment error of the document’s feature lines, which carries clear geometric significance. However, existing metrics fail to capture this characteristic effectively. We introduce the AAD (Axis-Aligned Distortion) metric, which quantifies distortion by measuring the axial alignment error of the dewarped results. The metric meaning is the same as in 3.1, the key difference is that this metric is computed during the evaluation phase using given image pairs rather than 2D grid pairs from the training phase.

Let  $y$  denote the ground truth image. The optical flow field from  $y$  to its dewarped version is computed using the SIFT-flow algorithm [20], yielding flow components  $v_x$  and  $v_y$  along the horizontal and vertical directions, respectively. The directional gradients of  $y$  are then extracted using the Sobel operator [29] along each axis and normalized:

$$\tilde{g}_i = \frac{|\text{Sobel}_i(y)|}{\max(|\text{Sobel}_i(y)|)}, \quad i \in \{x, y\}. \quad (12)$$

For each row  $i$  and column  $j$ , we compute the gradient-weighted means and the corresponding deviations as follows:

$$m_i = \frac{\sum_j v_y(i, j) \tilde{g}_y(i, j)}{\sum_j \tilde{g}_y(i, j) + \epsilon}, d_{i,j}^{\text{row}} = \tilde{g}_y(i, j) \cdot |v_y(i, j) - m_i|, \\ n_j = \frac{\sum_i v_x(i, j) \tilde{g}_x(i, j)}{\sum_i \tilde{g}_x(i, j) + \epsilon}, d_{i,j}^{\text{col}} = \tilde{g}_x(i, j) \cdot |v_x(i, j) - n_j|. \quad (13)$$

Here,  $m_i$  and  $n_j$  denote the gradient-weighted mean of the vertical flow in the  $i$ th row and the horizontal flow in the  $j$ th column, respectively, while  $d_{i,j}^{\text{row}}$  and  $d_{i,j}^{\text{col}}$  measure the corresponding deviations in pixel  $(i, j)$ .

Define the pixel-wise overall deviation as the Euclidean combination of the row and column deviations, and let the

<sup>1</sup><https://pypi.org/project/pytesseract/>

AAD be their average over all  $N$  pixels:

$$d_{i,j} = \sqrt{[d_{i,j}^{\text{row}}]^2 + [d_{i,j}^{\text{col}}]^2}, \text{AAD} = \frac{1}{N} \sum_{i,j} d_{i,j}. \quad (14)$$

The AAD metric uses the normalized image direction gradient weight to calculate the axial alignment error of the feature line in the row and column, lower values indicate a better dewarping effect.

Fig. 4 shows an example visualization of the AAD metric. For two different dewarped results, the alignment of table feature lines and the horizontal alignment of text lines serve as the primary evaluation criteria. By overlaying the horizontal and vertical components of the AAD heatmap onto the dewarped results, the corresponding axis alignment errors are displayed in detail. The heatmap colors correlate well with the calculated values, offering a perceptual measure of axis alignment.

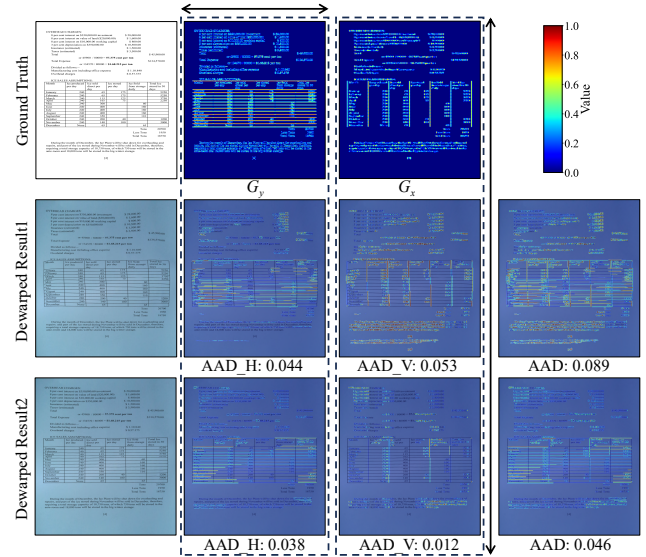


Figure 4. Example of visualizing AAD metrics. The first row is the ground truth image and its gradient heatmap in the horizontal ( $G_y$ ) and vertical ( $G_x$ ) directions; the second and third rows correspond to the two different dewarped results and their overlay heatmaps for AAD and its horizontal (AAD\_H) and vertical (AAD\_V) components, it can according to the  $\updownarrow$  and  $\leftrightarrow$  arrows to see the distortion error in the alignment direction of the corresponding axes.

To validate the robustness of the proposed AAD metric, we applied geometric and illumination disturbances to the dewarped images shown in Fig. 5, generating 100 warped images for each setting. The known disturbance serves as the optical flow information for calculating the ground truth metrics, while the optical flow information obtained via the SIFT-flow[20] method is used to compute the reference metrics. The linear correlation between the reference

value and the actual value of each metric can be a criterion for their robustness. As shown in Fig. 6(a), the AAD metric demonstrated the highest linear correlation ( $R^2$ ) across all sets, indicating a strong linear relationship with the ground truth even under minimal geometric disturbances (i.e., in regions with lower metric values, which are critical for comparing dewarped results that closely approximate the true values). In contrast, the AD metric exhibited a nonlinear response in these regions. In Fig. 6(b), we evaluated the normalized standard deviation under three different illumination conditions for each image in Fig. 5. The results revealed that the standard deviation for AAD (0.0230) was smaller than that for AD (0.0252), further confirming its enhanced robustness.

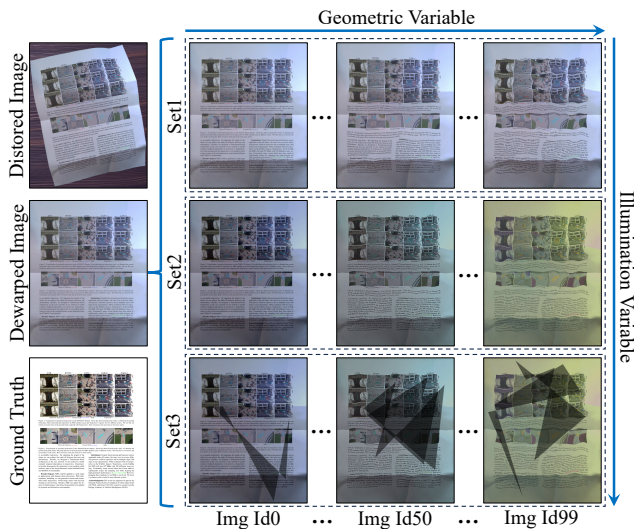


Figure 5. Geometric and illumination disturbances applied to the dewarped image. On the left is the distorted corresponding to the dewarped and ground truth images. On the right, geometric and illumination disturbances are added to the dewarped image, and the intensity increases along with the corresponding arrow direction. Set1 includes only geometric disturbances, Set2 adds color interference to Set1, and Set3 adds a random shadow to Set2.

### 4.3. Implementation Details

Our model is implemented using the PyTorch framework [28]. The dewarping model is trained on two datasets: Doc3D [5] (88k images) and UVDoc [36] (20k images). The input images are resized to  $712 \times 488$  pixels, while the output 2D grid is set to  $45 \times 31$ . We optimize the model using the AdamW optimizer [21] with a batch size of 72. The initial learning rate is  $1 \times 10^{-5}$  and is linearly decayed to 0 during training. The network is trained for 30 epochs on two NVIDIA 4090 GPUs, which takes approximately 15 hours. During inference (see Sec. 3.3), a single round of preprocessing is applied for the DocUNet and UVDoc benchmarks, whereas for the DIR300 benchmark—with its

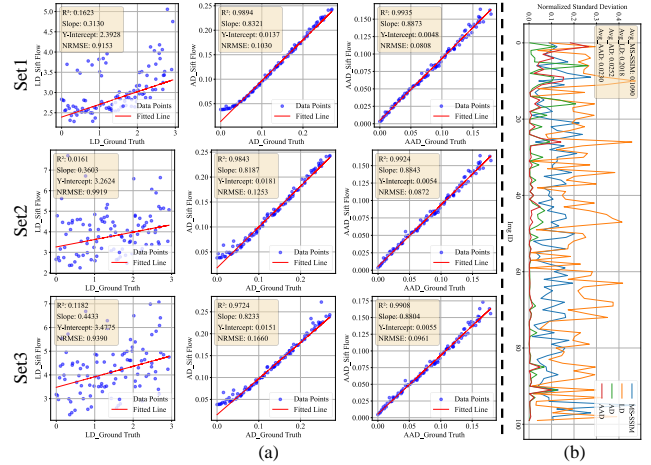


Figure 6. Robustness analysis of each metric. (a) The x-axis represents the ground truth metric computed from the ground truth optical flow, while the y-axis represents the reference metric derived from the SIFT-flow method; ideally, they should exhibit a high linear correlation. (b) The normalized standard deviation of the metrics under three different environmental conditions, lower values indicate greater robustness to environmental disturbances.

smaller target objects—preprocessing is performed twice.

### 4.4. Experimental Results

We compare our method against existing approaches both quantitatively and qualitatively on the aforementioned benchmarks.

Table 1. Quantitative evaluation on the DocUNet benchmark [23]. We compare our method with existing methods in terms of Multi-Scale Structural Similarity (MS), Local Distortion (LD), Aligned Distortion (AD), Axis-Aligned Distortion (AAD), Character Error Rate (CER) and Edit Distance (ED), “↑” indicates the higher the better and “↓” means the opposite, Bold font denotes the best result, and underline indicates second-best. The “Improvements” row shows the relative gain of our metric over the previous best.

Method	MS↑	LD↓	AD↓	AAD↓	ED↓	CER↓
DewarpNet[5]	0.474	8.362	0.398	0.164	824.5	0.225
DDCP[40]	0.472	8.982	0.428	0.159	1124.7	0.280
DocTr[7]	0.509	7.773	0.369	0.151	708.6	0.185
PaperEdge[24]	0.473	7.967	0.368	<u>0.121</u>	731.4	0.183
DocGeoNet[8]	0.504	7.717	0.381	0.158	695.0	0.187
FAM[16]	0.497	8.416	0.377	0.151	<u>688.3</u>	<u>0.176</u>
Layout[17]	0.525	<u>6.706</u>	<u>0.300</u>	0.121	689.8	0.180
UVDoc[36]	<b>0.545</b>	6.827	0.316	0.125	754.2	0.193
<b>Ours</b>	<u>0.543</u>	<b>6.249</b>	<b>0.278</b>	<b>0.099</b>	<b>603.1</b>	<b>0.150</b>
<b>Improvements</b>	-0.4%	6.8%	7.3%	18.2%	12.4%	14.8%

In Tab. 1, we compare our method with previous approaches on the DocUNet benchmark. Our approach demonstrates significant improvements across most metrics and achieves performance comparable to UVDoc [36]



Figure 7. Qualitative evaluation on the DocUNet benchmark. The figure shows the dewarped results along with the corresponding heatmap overlays of the AAD component metric. The horizontal ( $\leftrightarrow$ ) and vertical ( $\updownarrow$ ) arrows indicate the directions for visualizing the axis-aligned error of the dewarped feature lines.

on the MS metric. Notably, our method delivers an 18.2% improvement on the proposed AAD metric. Furthermore, we performed a qualitative analysis of global images (see Fig. 7) by selecting several test cases rich in horizontal and vertical features for dewarping comparison. To highlight the distortion areas more clearly, we overlay the dewarped results from different methods with heatmaps generated from the horizontal and vertical components of the proposed AAD metric (an example is provided in Fig. 4). For our method, the resulting heatmaps appear fainter on documents with feature lines in varying orientations, indicating a reduced axis alignment error. As expected from the dewarping results in Fig. 1, the feature lines exhibit improved axis alignment in the dewarped images.

Table 2. Quantitative evaluation on the DIR300 benchmark[8]. The evaluation protocol is identical to that described in Tab. 1.

Method	MS $\uparrow$	LD $\downarrow$	AD $\downarrow$	AAD $\downarrow$	ED $\downarrow$	CER $\downarrow$
DewarpNet[5]	0.492	13.944	0.332	0.147	1076.8	0.336
DDCP[40]	0.552	11.02	0.357	0.132	739.3	0.257
DocTr[7]	0.616	7.189	0.255	0.107	698.4	0.211
PaperEdge[24]	0.584	7.968	0.255	0.091	447.4	0.177
DocGeoNet[8]	0.638	6.403	0.241	0.106	672.5	0.206
FAM[16]	0.607	7.680	0.243	0.108	639.4	0.198
Layout[17]	0.652	5.702	0.195	0.087	495.4	0.173
UVDoc[36]	0.621	7.730	0.219	0.101	614.0	0.237
<b>Ours</b>	<b>0.702</b>	<b>4.261</b>	<b>0.131</b>	<b>0.057</b>	<b>405.8</b>	<b>0.132</b>
<b>Improvements</b>	7.7%	25.3%	32.8%	34.5%	9.3%	23.7%

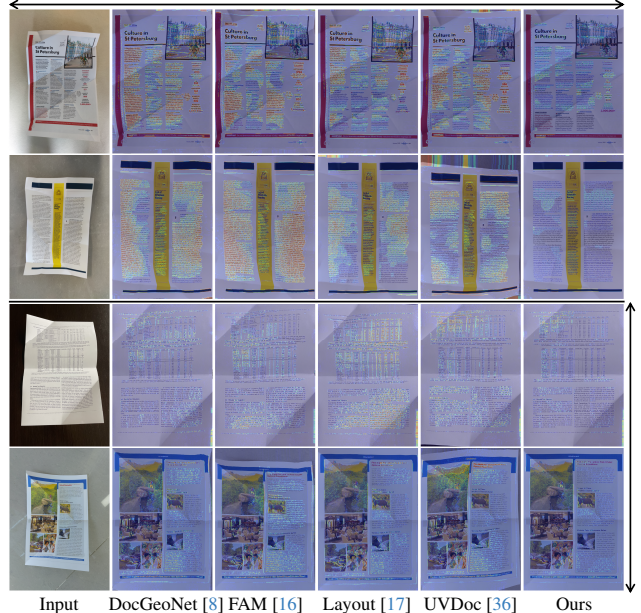


Figure 8. Qualitative evaluations on the DIR300 benchmark. We compare our method with existing methods as described in Fig. 7.

In Tab. 2, we evaluate our method on the DIR300 benchmark, which comprises 300 images—the largest among the three benchmarks. Our approach achieves notable improvements across all metrics, with the AAD metric improvement to 34.5%. Furthermore, the dewarped results significantly boost OCR performance, with the CER reaching 23.7%. These improvements are qualitatively demonstrated in Fig. 8. Our method substantially reduces the distortion of document feature lines, resulting in fainter heatmap colors and yielding more complete and straighter contours.

Table 3. Quantitative evaluation on the UVDoc benchmark [36]. The evaluation protocol is identical to that described in Tab. 1.

Method	MS $\uparrow$	LD $\downarrow$	AD $\downarrow$	AAD $\downarrow$	ED $\downarrow$	CER $\downarrow$
DewarpNet[5]	0.589	<b>5.666</b>	0.193	0.085	297.8	0.117
DDCP[40]	0.585	11.582	0.290	0.109	251.8	0.094
DocTr[7]	0.697	8.146	0.161	0.075	<u>110.8</u>	<b>0.034</b>
DocGeoNet[8]	0.706	8.350	0.168	0.072	123.1	0.047
RDGR[12]	0.610	6.423	0.281	0.096	122.45	0.051
UVDoc[36]	<u>0.785</u>	6.810	<u>0.119</u>	<u>0.052</u>	122.7	0.046
<b>Ours</b>	<b>0.800</b>	<u>5.834</u>	<b>0.098</b>	<b>0.040</b>	<b>104.3</b>	<u>0.036</u>
<b>Improvements</b>	1.9%	-3.0%	17.6%	23.1%	5.9%	-5.9%

In Tab. 3, we present the quantitative results on the UVDoc benchmark. Our method outperforms competing approaches across all metrics except for LD and CER, where our results are very close to the best values. Notably, the AAD metric improves by 23.1%. In the qualitative comparison shown in Fig. 9, dewarped results in both horizontal and vertical directions are displayed. These comparisons reveal that our method achieves excellent axis-aligned de-

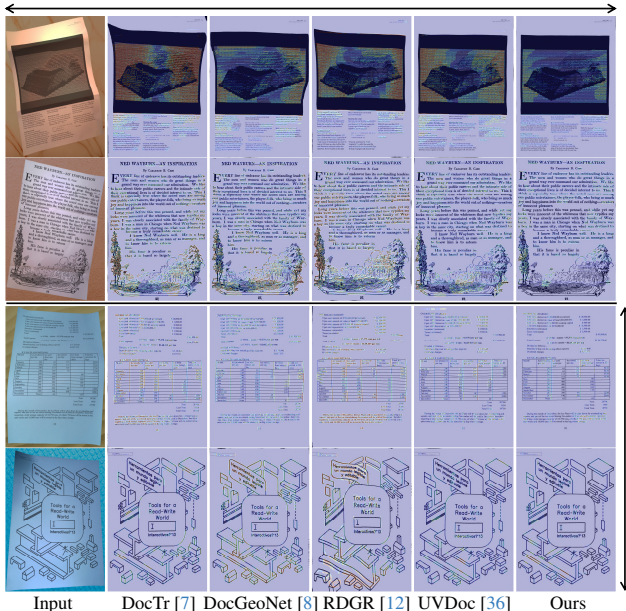


Figure 9. Qualitative comparisons on the UVDoc benchmark. We compare our method with existing methods as described in Fig. 7.

warping performance even in regions without textual features, highlighting the superiority of our approach.

#### 4.5. Ablation Study

We conducted ablation experiments to evaluate the impact of two key components: the axis-aligned geometric constraint used during training (Sec. 3.1) and the axis alignment preprocessing applied during inference (Sec. 3.3).

As summarized in Tab. 4, both components independently enhance performance across three benchmark datasets. Specifically, for the DocUNet and UVDoc benchmarks—where a large proportion of targets are present—the axis-aligned geometric constraint yields greater performance improvements than the axis alignment preprocessing. Conversely, in the DIR300 benchmark, which contains a smaller proportion of targets, the benefits of the preprocessing strategy are more pronounced. Importantly, the combination of both modules produces the best overall performance, demonstrating their complementary advantages in different scenarios.

Fig. 10 provides several examples from our ablation experiments. For targets with a smaller proportion (middle row), the preprocessing strategy improves target integrity, while the addition of the axis-aligned geometric constraint further enhances the de-warping performance. For targets with a larger proportion (first and last rows), the performance gains from the axis-aligned geometric constraint are more prominent. Overall, the optimal de-warped results are achieved by applying both components simultaneously, which aligns with the improvements observed in the quali-

Table 4. Ablation study on various benchmarks. We evaluate the impact of the axis-aligned geometric constraint loss (AL) and the axis alignment preprocessing strategy (AP) module. The symbols  $\times$  and  $\checkmark$  indicate that the corresponding module is disabled or enabled, respectively. Bold font denotes the best performance, while underline values indicate the second-best scores.

Benchmark	AL	AP	MS $\uparrow$	LD $\downarrow$	AD $\downarrow$	AAD $\downarrow$	ED $\downarrow$	CER $\downarrow$
DocUNet[23]	$\times$	$\times$	0.538	6.897	0.322	0.124	638.1	0.167
	$\checkmark$	$\times$	<b>0.549</b>	<u>6.566</u>	<u>0.291</u>	<u>0.105</u>	718.0	0.183
	$\times$	$\checkmark$	0.536	6.767	0.308	0.120	<u>628.5</u>	<u>0.165</u>
	$\checkmark$	$\checkmark$	<u>0.543</u>	<b>6.249</b>	<b>0.278</b>	<b>0.099</b>	<b>603.1</b>	<b>0.150</b>
DIR300[8]	$\times$	$\times$	0.615	7.691	0.215	0.100	633.0	0.243
	$\checkmark$	$\times$	0.629	7.880	0.176	0.076	<u>498.9</u>	0.206
	$\times$	$\checkmark$	0.694	<u>4.303</u>	<u>0.152</u>	<u>0.069</u>	541.6	<u>0.153</u>
	$\checkmark$	$\checkmark$	<b>0.702</b>	<b>4.261</b>	<b>0.131</b>	<b>0.057</b>	<b>405.8</b>	<b>0.132</b>
UVDoc[36]	$\times$	$\times$	0.794	6.356	0.118	0.052	120.4	0.041
	$\checkmark$	$\times$	0.785	<u>5.903</u>	0.116	<u>0.044</u>	<u>105.2</u>	<b>0.035</b>
	$\times$	$\checkmark$	0.790	6.024	<u>0.111</u>	0.049	118.2	0.043
	$\checkmark$	$\checkmark$	<b>0.800</b>	<b>5.834</b>	<b>0.098</b>	<b>0.040</b>	<b>104.3</b>	<u>0.036</u>

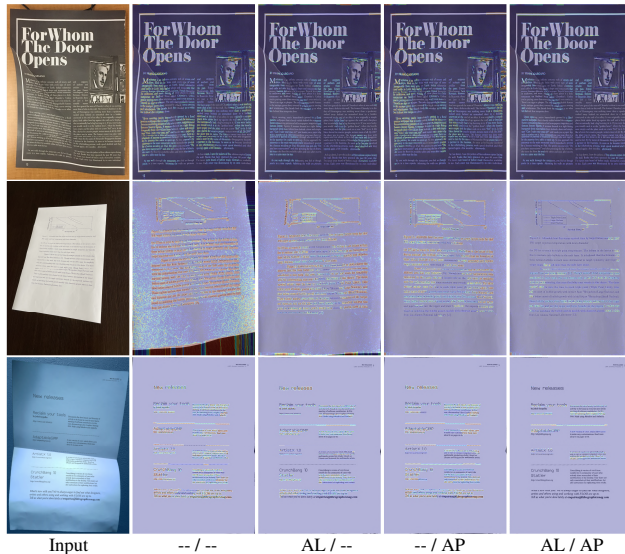


Figure 10. De-warped results under different ablation settings. From left to right, each row displays the distorted input image followed by the de-warped outputs generated by different ablation settings. The heatmap value is the horizontal component of the AAD metric.

tative metrics in Tab. 4.

## 5. Conclusion

This paper proposes a document de-warping method that exploits the inherent axis-aligned properties of planar documents’ discrete grid geometry. By incorporating an axis-aligned geometric constraint during network training and applying an axis alignment preprocessing step during inference, our method outperforms state-of-the-art methods across multiple benchmarks. Experimental results

demonstrate that these components are both independently effective and complementary. We also introduce a novel metric, AAD, which offers a clear geometric interpretation, aligns well with human visual perception, and exhibits enhanced robustness. Unlike previous studies that primarily focus on network architecture or dataset contributions, our approach leverages the intrinsic geometry of documents to improve dewarping performance. Future work will further explore these geometric properties and extend their application to other image dewarping tasks.

## References

- [1] Michael S Brown and W Brent Seales. Document restoration using 3d shape: a general deskewing algorithm for arbitrarily warped documents. In *Proceedings Eighth IEEE International Conference on Computer Vision. ICCV 2001*, pages 367–374. IEEE, 2001. 1
- [2] Michael S Brown and Y-C Tsoi. Geometric and shading correction for images of printed materials using boundary. *IEEE Transactions on Image Processing*, 15(6):1544–1554, 2006. 1
- [3] Huaigu Cao, Xiaoqing Ding, and Changsong Liu. A cylindrical surface model to rectify the bound document image. In *Proceedings Ninth IEEE international conference on computer vision*, pages 228–233. IEEE, 2003. 2
- [4] Beiya Dai, Qunyi Xie, Yulin Li, Xiameng Qin, Chengquan Zhang, Kun Yao, Junyu Han, et al. Matadoc: margin and text aware document dewarping for arbitrary boundary. *arXiv preprint arXiv:2307.12571*, 2023. 2
- [5] Sagnik Das, Ke Ma, Zhixin Shu, Dimitris Samaras, and Roy Shilkrot. Dewarpnet: Single-image document unwarping with stacked 3d and 2d regression networks. In *Proceedings of the IEEE/CVF international conference on computer vision*, pages 131–140, 2019. 1, 2, 4, 6, 7
- [6] Sagnik Das, Kunwar Yashraj Singh, Jon Wu, Erhan Bas, Vijay Mahadevan, Rahul Bhotika, and Dimitris Samaras. End-to-end piece-wise unwarping of document images. In *Proceedings of the IEEE/CVF International Conference on Computer Vision*, pages 4268–4277, 2021.
- [7] Hao Feng, Yuechen Wang, Wengang Zhou, Jiajun Deng, and Houqiang Li. Doctr: Document image transformer for geometric unwarping and illumination correction. In *Proceedings of the 29th ACM International Conference on Multimedia*, pages 273–281, 2021. 1, 2, 4, 6, 7, 8
- [8] Hao Feng, Wengang Zhou, Jiajun Deng, Yuechen Wang, and Houqiang Li. Geometric representation learning for document image rectification. In *European Conference on Computer Vision*, pages 475–492. Springer, 2022. 1, 2, 4, 6, 7, 8
- [9] Yuan He, Pan Pan, Shufu Xie, Jun Sun, and Satoshi Naoi. A book dewarping system by boundary-based 3d surface reconstruction. In *2013 12th international conference on document analysis and recognition*, pages 403–407. IEEE, 2013. 2
- [10] Felix Hertlein, Alexander Naumann, and Patrick Philipp. Inv3d: a high-resolution 3d invoice dataset for template-guided single-image document unwarping. *International Journal on Document Analysis and Recognition (IJDAR)*, 2023. 2
- [11] Caigui Jiang, Cheng Wang, Florian Rist, Johannes Wallner, and Helmut Pottmann. Quad-mesh based isometric mappings and developable surfaces. *ACM Transactions on Graphics (TOG)*, 39(4):128–1, 2020. 2
- [12] Xiangwei Jiang, Rujiao Long, Nan Xue, Zhibo Yang, Cong Yao, and Gui-Song Xia. Revisiting document image dewarping by grid regularization. In *Proceedings of the IEEE/CVF Conference on Computer Vision and Pattern Recognition*, pages 4543–4552, 2022. 1, 2, 7, 8
- [13] Taeho Kil, Wonkyo Seo, Hyung Il Koo, and Nam Ik Cho. Robust document image dewarping method using text-lines and line segments. In *2017 14th IAPR international conference on document analysis and recognition (ICDAR)*, pages 865–870. IEEE, 2017. 1
- [14] Beom Su Kim, Hyung Il Koo, and Nam Ik Cho. Document dewarping via text-line based optimization. *Pattern Recognition*, 48(11):3600–3614, 2015. 1, 2
- [15] VI Levenshtein. Binary codes capable of correcting deletions, insertions, and reversals. *Proceedings of the Soviet physics doklady*, 1966. 5
- [16] Heng Li, Xiangping Wu, Qingcai Chen, and Qianjin Xiang. Foreground and text-lines aware document image rectification. In *Proceedings of the IEEE/CVF International Conference on Computer Vision*, pages 19574–19583, 2023. 1, 2, 6, 7
- [17] Pu Li, Weize Quan, Jianwei Guo, and Dong-Ming Yan. Layout-aware single-image document flattening. *ACM Transactions on Graphics*, 43(1):1–17, 2023. 1, 2, 6, 7
- [18] Xiaoyu Li, Bo Zhang, Jing Liao, and Pedro V Sander. Document rectification and illumination correction using a patch-based cnn. *ACM Transactions on Graphics (TOG)*, 38(6):1–11, 2019. 2
- [19] Jian Liang, Daniel DeMenthon, and David Doermann. Geometric rectification of camera-captured document images. *IEEE transactions on pattern analysis and machine intelligence*, 30(4):591–605, 2008. 1, 2
- [20] Ce Liu, Jenny Yuen, and Antonio Torralba. Sift flow: Dense correspondence across scenes and its applications. *IEEE transactions on pattern analysis and machine intelligence*, 33(5):978–994, 2010. 5
- [21] I Loshchilov. Decoupled weight decay regularization. *arXiv preprint arXiv:1711.05101*, 2017. 6
- [22] Dong Luo and Pengbo Bo. Geometric rectification of creased document images based on isometric mapping. *arXiv preprint arXiv:2212.08365*, 2022. 2
- [23] Ke Ma, Zhixin Shu, Xue Bai, Jue Wang, and Dimitris Samaras. Docunet: Document image unwarping via a stacked u-net. In *Proceedings of the IEEE conference on computer vision and pattern recognition*, pages 4700–4709, 2018. 1, 2, 4, 5, 6, 8
- [24] Ke Ma, Sagnik Das, Zhixin Shu, and Dimitris Samaras. Learning from documents in the wild to improve document unwarping. In *ACM SIGGRAPH 2022 Conference Proceedings*, pages 1–9, 2022. 1, 4, 5, 6, 7

- [25] Amir Markovitz, Inbal Lavi, Or Perel, Shai Mazor, and Roei Litman. Can you read me now? content aware rectification using angle supervision. In *Computer Vision—ECCV 2020: 16th European Conference, Glasgow, UK, August 23–28, 2020, Proceedings, Part XII 16*, pages 208–223. Springer, 2020. 1
- [26] Gaofeng Meng, Ying Wang, Shenquan Qu, Shiming Xiang, and Chunhong Pan. Active flattening of curved document images via two structured beams. In *Proceedings of the IEEE Conference on Computer Vision and Pattern Recognition*, pages 3890–3897, 2014. 1, 2
- [27] Andrew Cameron Morris, Viktoria Maier, and Phil D Green. From wer and ril to mer and wil: improved evaluation measures for connected speech recognition. In *Interspeech*, pages 2765–2768, 2004. 5
- [28] Adam Paszke, Sam Gross, Soumith Chintala, Gregory Chanan, Edward Yang, Zachary DeVito, Zeming Lin, Alban Desmaison, Luca Antiga, and Adam Lerer. Automatic differentiation in pytorch. 2017. 6
- [29] Irwin Sobel, Gary Feldman, et al. A 3x3 isotropic gradient operator for image processing. *a talk at the Stanford Artificial Project in*, 1968:271–272, 1968. 5
- [30] Nikolaos Stamatopoulos, Basilis Gatos, Ioannis Pratikakis, and Stavros J Perantonis. Goal-oriented rectification of camera-based document images. *IEEE transactions on image processing*, 20(4):910–920, 2010. 2
- [31] Yusuke Takezawa, Makoto Hasegawa, and Salvatore Tabbone. Robust perspective rectification of camera-captured document images. In *2017 14th IAPR International Conference on Document Analysis and Recognition (ICDAR)*, pages 27–32. IEEE, 2017. 2
- [32] Chew Lim Tan, Li Zhang, Zheng Zhang, and Tao Xia. Restoring warped document images through 3d shape modeling. *IEEE Transactions on Pattern Analysis and Machine Intelligence*, 28(2):195–208, 2005. 2
- [33] Yau-Chat Tsoi and Michael S Brown. Multi-view document rectification using boundary. In *2007 IEEE Conference on Computer Vision and Pattern Recognition*, pages 1–8. IEEE, 2007. 1
- [34] Adrian Ulges, Christoph H Lampert, and Thomas Breuel. Document capture using stereo vision. In *Proceedings of the 2004 ACM symposium on Document engineering*, pages 198–200, 2004. 1
- [35] Adrian Ulges, Christoph H Lampert, and Thomas M Breuel. Document image dewarping using robust estimation of curled text lines. In *Eighth International Conference on Document Analysis and Recognition (ICDAR’05)*, pages 1001–1005. IEEE, 2005. 2
- [36] Floor Verhoeven, Tanguy Magne, and Olga Sorkine-Hornung. Uvdoc: Neural grid-based document unwarping. In *SIGGRAPH Asia 2023 Conference Papers*, pages 1–11, 2023. 1, 2, 3, 4, 6, 7, 8
- [37] Toshikazu Wada, Hiroyuki Ukida, and Takashi Matsuyama. Shape from shading with interreflections under a proximal light source: Distortion-free copying of an unfolded book. *International Journal of Computer Vision*, 24:125–135, 1997. 2
- [38] Chaoyun Wang, Jingmin Xin, Nanning Zheng, and Caigui Jiang. Gso-net: Grid surface optimization via learning geometric constraints. In *Proceedings of the AAAI Conference on Artificial Intelligence*, pages 8163–8171, 2024. 2
- [39] Guo-Wang Xie, Fei Yin, Xu-Yao Zhang, and Cheng-Lin Liu. Dewarping document image by displacement flow estimation with fully convolutional network. In *Document Analysis Systems: 14th IAPR International Workshop, DAS 2020, Wuhan, China, July 26–29, 2020, Proceedings 14*, pages 131–144. Springer, 2020. 1, 2
- [40] Guo-Wang Xie, Fei Yin, Xu-Yao Zhang, and Cheng-Lin Liu. Document dewarping with control points. In *Document Analysis and Recognition—ICDAR 2021: 16th International Conference, Lausanne, Switzerland, September 5–10, 2021, Proceedings, Part I 16*, pages 466–480. Springer, 2021. 1, 2, 6, 7
- [41] Fangchen Yu, Yina Xie, Lei Wu, Yafei Wen, Guozhi Wang, Shuai Ren, Xiaoxin Chen, Jianfeng Mao, and Wenye Li. Docreal: Robust document dewarping of real-life images via attention-enhanced control point prediction. In *Proceedings of the IEEE/CVF Winter Conference on Applications of Computer Vision*, pages 665–674, 2024. 1
- [42] Jiaxin Zhang, Canjie Luo, Lianwen Jin, Fengjun Guo, and Kai Ding. Marior: Margin removal and iterative content rectification for document dewarping in the wild. In *Proceedings of the 30th ACM International Conference on Multimedia*, pages 2805–2815, 2022. 2
- [43] Li Zhang, Andy M Yip, Michael S Brown, and Chew Lim Tan. A unified framework for document restoration using inpainting and shape-from-shading. *Pattern Recognition*, 42(11):2961–2978, 2009. 2